In-beam γ-ray spectroscopy of neutron-rich boron isotopes ^{15,17}B via inelastic scattering on ^{12}C

Y. Kondo,[1] T. Nakamura,[1] N. Aoi,[2] H. Baba,[3] D. Bazin,[4] N. Fukuda,[2] T. Gomi,[2] H. Hasegawa,[5] N. Imai,[2] M. Ishihara,[2] T. Kobayashi,[6] T. Kubo,[2] M. Miura,[1] T. Motobayashi,[2] A. Saito,[3] H. Sakurai,[7] S. Shimoura,[3] T. Sugimoto,[1] K. Watanabe,[6] Y. X. Watanabe,[8] T. Yakushiji,[6] Y. Yanagisawa,[2] and K. Yoneda[4]

[1]*Department of Physics, Tokyo Institute of Technology, 2-12-1 Oh-Okayama, Meguro, Tokyo 152-8551, Japan*

[2]*Institute of Physical and Chemical Research (RIKEN), Hirosawa 2-1, Wako, Saitama 351-0198, Japan*

[3]*Center for Nuclear Study (CNS), University of Tokyo, RIKEN campus, Hirosawa 2-1, Wako, Saitama 351-0198, Japan*

[4]*National Superconducting Cyclotron Laboratory, Michigan State University, 1 Cyclotron, East Lansing, Michigan 48824-1321, USA*

[5]*Department of Physics, Rikkyo University, Nishi-Ikebukuro 3-34-1, Toshima, Tokyo 171-8501, Japan*

[6]*Department of Physics, Tohoku University, Katahira 2-1-1, Aoba, Sendai, Miyagi 980-8577, Japan*

[7]*Department of Physics, University of Tokyo, Hongo 7-3-1, Bunkyo, Tokyo 113-0033, Japan*

[8]*High Energy Accelerator Research Organization (KEK), Oho 1-1, Tsukuba, Ibaraki 305-0801, Japan*

(Received 3 September 2004; published 28 April 2005)

Low-lying bound states of the neutron-rich boron isotopes, ^{15}B and ^{17}B, have been investigated using the ^{15,17}B + ^{12}C inelastic scatterings at approximately 70 MeV/nucleon. In-beam γ-ray spectroscopy was used to determine the energy levels of the excited states, and the angular distribution of the particle in the inelastic channel populating each state was measured. Two bound states were observed for ^{15}B, while a new bound excited state was found for ^{17}B at $E_x = 1.07(1)$ MeV very close to the neutron emission threshold ($S_{2n} = 1.39$ MeV). The angular distributions for the transitions to these states are well reproduced with $\Delta L^\pi = 2^+$ diffraction patterns. The energy levels and $\Delta L^\pi = 2^+$ are consistent with shell model predictions. The quadrupole deformation lengths for the transitions extracted from the differential cross sections are compared to the shell model, suggesting a strong quenching of the neutron effective charge both for ^{15}B and ^{17}B.

DOI: 10.1103/PhysRevC.71.044611 PACS number(s): 21.10.Re, 23.20.Lv, 25.60.−t, 27.20.+n

I. INTRODUCTION

Neutron-rich boron isotopes have recently drawn much attention because of their exotic structures. ^{17}B is a loosely bound Borromean nucleus, as ^{16}B is unbound and its $2n$ separation energy S_{2n} is only 1.39 MeV [1]. A two-neutron halo structure in ^{17}B has been experimentally suggested from the large rms radius determined from the measurements of reaction and total interaction cross sections [2–4], as well as from the narrow momentum distribution of ^{15}B observed in the $2n$ breakup of ^{17}B [5]. The halo structure of ^{17}B was studied theoretically as well [6,7]. Further insight was found in the measurement of the quadrupole moments of ^{15}B and ^{17}B [8,9], where a strong quenching of the neutron effective charge was suggested. This effect may be related to the decoupling of the valence neutrons as suggested in the neighboring neutron-rich nucleus ^{16}C [10,11]. In terms of the cluster model, the Li-He clustering structure was predicted to develop with an increase in the neutron number in the framework of antisymmetrized molecular dynamics (AMD) [12]. In spite of these results, there have been only a few experimental studies on the excited states of ^{15}B and ^{17}B. A multinucleon transfer reaction [13] revealed excited levels in ^{15}B above the neutron emission threshold ($S_n = 2.77$ MeV [14,15]). More recently, two bound states in ^{15}B were observed using a fragmentation reaction of ^{36}S on a ^{9}Be target [16]. For ^{17}B, so far no excited states have been reported experimentally.

We have studied bound excited states of ^{15}B and ^{17}B using the technique of in-beam γ-ray spectroscopy applied to the inelastic scattering on ^{12}C. In-beam γ-ray spectroscopy with an intermediate-energy radioactive ion beam offers a powerful spectroscopic tool for a broad range of unstable nuclei extending up to the drip line. In this technique, γ rays from an excited state of the ejectile are measured in coincidence with the ejectile. The γ-ray energy is determined precisely by correcting for the Doppler shift. The advantage of in-beam γ-ray spectroscopy with an intermediate-energy radioactive ion beam is a large yield of γ rays measured in coincidence with the ejectile because of the availability of a thick target as well as the kinematic focusing of the ejectile. Combined with the in-beam γ-ray technique, several reactions, such as Coulomb excitation with a heavy target, two-step fragmentation reaction, and inelastic scattering with a light target, have been successfully used to investigate the properties of radioactive nuclei. For instance, Coulomb excitation has been used to obtain the $B(E2 : 0^+_{\text{g.s.}} \rightarrow 2^+_1)$ value in ^{32}Mg to clarify the break of magicity at $N = 20$ [17]. Coulomb excitation has also been applied to a wide range of neutron-rich nuclei [18–20]. Two-step fragmentation was used to observe bound excited states in neutron-rich isotopes [21,22]. Two-step fragmentation, which basically has no selection rule for the states populated, provides a better access to higher excited states such as $J^\pi = 4^+$ for even-even nuclei. In-beam γ-ray spectroscopy with proton inelastic scattering revealed a large quadrupole deformation length for ^{12}Be [23] despite the fact that ^{12}Be is an $N = 8$ nucleus. Proton inelastic scattering was also applied to the $N = 20$ nucleus ^{30}Ne, which led to the observation of its first excited state [24], with its energy providing evidence that this nucleus is within the "island of inversion."

In the present study, we used ^{12}C as a target. Since it is a $T = 0$ target and the charge of the nucleus is small, we expect primarily isoscalar nuclear transitions with this target. The ^{12}C nucleus offers an alternative to the ideal $T = 0$ probe ^{4}He and is easier to handle than ^{4}He. The use of a $T = 0$ target is suitable for the present case because all the low-lying bound states of ^{15}B and ^{17}B predicted by shell models and cluster models are accessible by $\Delta L = 2^+$, $\Delta T = 0$ transitions (see the predicted levels later in Figs. 3 and 6). The main focus of the present experiment is the angular distributions of the inelastically scattered particle, associated with a specific γ ray. The ^{12}C target as an inelastic probe for radioactive nuclei has so far been applied only to angle-integrated cross sections [25]. Differential cross sections obtained in the present experiment can be compared directly to distorted-wave Born approximation (DWBA) calculations to extract the spin-parity of the transition, as well as the associated deformation lengths. These are then compared to the transition matrix elements calculated by a shell model, giving useful structure information on the low-lying states of ^{15}B and ^{17}B. We also measured γ rays in the multineutron removal reactions of ^{15}B and ^{17}B into ^{12,14,15}B for calibration purposes.

The paper is organized as follows. Section II describes the experimental setup. In Sec. III, the experimental results are presented, and the observed γ rays of ^{15,17}B are shown as well as the associated scattering angular distributions. In Sec. IV, these results are compared with the shell model calculations to discuss the effective charge of these nuclei. Then conclusions are given in Sec. V.

II. EXPERIMENT

The experiment was performed at the RIKEN Accelerator Research Facility using the in-flight radioactive-isotope beam separator, RIPS [26]. A ^{22}Ne beam at 110 MeV/nucleon bombarded a primary Be target of thickness 1.1 g/cm^2 to produce the secondary ^{15}B and ^{17}B beams. The intensities of the secondary beams selected by RIPS were 1.2×10^4 counts per second for ^{15}B and 8.2×10^2 counts per second for ^{17}B. The ^{15}B and ^{17}B beams of purities close to 90% were delivered to the experimental setup shown schematically in Fig. 1.

The particle identification of the secondary beam was performed event-by-event using the time-of-flight (TOF) information provided by the cyclotron radio frequency and a plastic scintillator of 1 mm thickness, located 5.5 m upstream of the secondary target. The thickness of the secondary ^{12}C target was 377 mg/cm^2. The average kinetic energies of the ^{15}B and ^{17}B beams were 72 MeV/nucleon at the middle of the target. The position and angle of the incident beam at the secondary target were obtained by using the position information from two parallel-plate avalanche counters (PPACs) [27]. The incident angle information is used to extract the scattering angle.

The outgoing boron isotopes were analyzed using a magnetic spectrometer equipped with a drift chamber (FDC3) and a plastic scintillator hodoscope. The particle identification of the outgoing boron isotopes was performed by combining the ΔE and TOF information from the hodoscope with the magnetic rigidity information from FDC3. The momentum vector of the outgoing particle was reconstructed from tracking analysis using the position and angle information from FDC3 and the TOF from the hodoscope. The angle of the outgoing particle at the secondary target was then deduced from the momentum vector. The incident and outgoing angles were combined to extract the scattering angle $\theta_{\text{c.m.}}$ in the c.m. frame of the projectile and target. The angular resolution was 1.44 (1.52) degrees (full width at half maximum, FWHM) in the c.m. frame for the ^{15}B (^{17}B) scattering on the ^{12}C target. The acceptance of the spectrometer was estimated using a Monte Carlo simulation. The acceptance was close to 100% up to $\theta_{\text{c.m.}} = 6^\circ$ (4°), and gradually decreased to about 50 (40)% at $\theta_{\text{c.m.}} = 10^\circ$ for the ^{15}B (^{17}B) scattering.

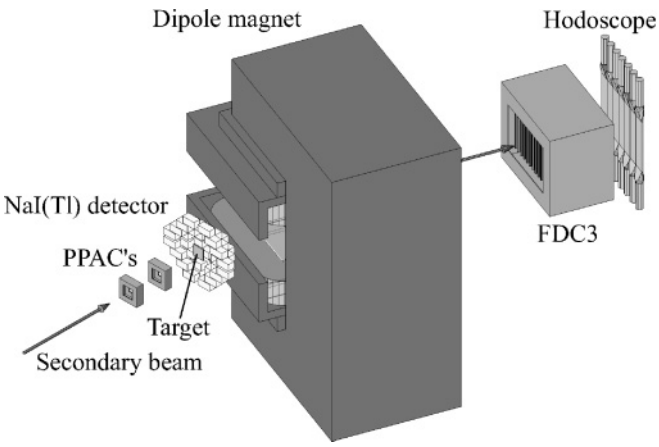

FIG. 1. Schematic view of the experimental setup around the final achromatic focal plane of RIPS. NaI(Tl) detectors are placed surrounding the secondary ^{12}C target. Inelastically scattered particles are analyzed with the spectrometer equipped with a drift chamber (FDC3) and a plastic scintillator hodoscope.

Deexcitation γ rays were detected using about a half-set of the DALI system [17], composed of 36 blocks of NaI(Tl) scintillators surrounding the secondary target. Each scintillator crystal has a size of $6 \times 6 \times 12$ cm^3. The high granularity of the setup provides the γ-ray emission angle with about 20° accuracy. The information of the angle of the γ-ray emission and velocity of the ejectile ($\beta \approx 0.37$) was used to correct for the large Doppler shift. The energy calibration was obtained using ^{22}Na, ^{60}Co, and ^{137}Cs γ sources. The uncertainty of the energy calibration was estimated to be 3 keV. The energy resolution was 12% (FWHM) for an in-flight γ ray at 1.07 MeV, due to the finite angular resolution, the uncertainty of the beam velocity at the reaction point in the thick target, and the intrinsic energy resolution of the detector. The photo-peak efficiency of the NaI(Tl) scintillators was estimated from a simulation using the GEANT code [28] to be 13% for a 1.07 MeV γ ray.

III. RESULTS

A. Energy spectra of γ rays

Figures 2(a) and 2(b) show the Doppler-corrected energy spectra of γ rays associated with inelastically scattered ^{17}B and ^{15}B on the ^{12}C target, respectively. To suppress the background due to Compton scattering events, we have

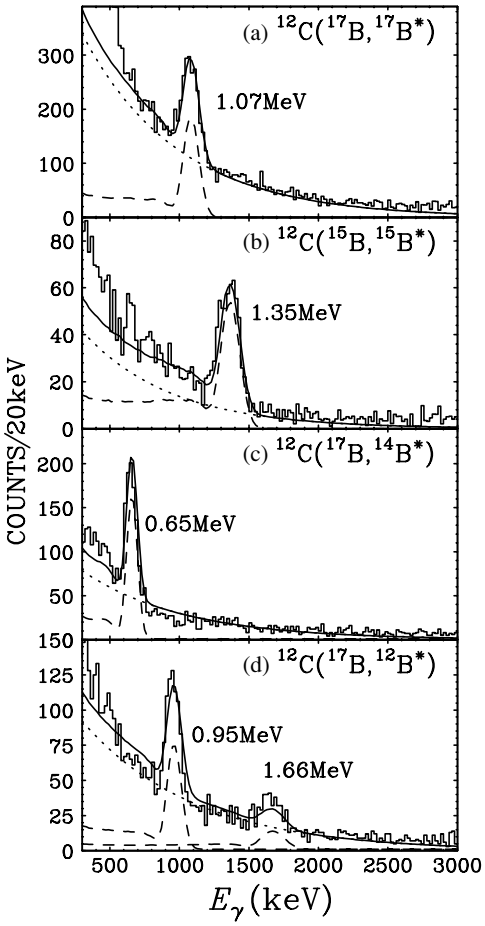

FIG. 2. Doppler-corrected energy spectra of the γ ray in coincidence with inelastically scattered ^{17}B (a) and ^{15}B (b) on ^{12}C, and with ^{14}B (c) and ^{12}B (d) produced from the breakup of ^{17}B. The solid lines show the results of a fit to the data by the simulated spectrum (dashed lines) with an exponential background (dotted lines) in order to deduce the γ-ray yield. For ^{15}B, the observed peak at 1.35 MeV contains two γ transitions.

selected the events with multiplicity [the number of the NaI(Tl) scintillators detecting a γ ray] equal to 1. A peak at 1.07(1) MeV associated with ^{17}B is observed for the first time. For ^{15}B, a peak at 1.35(1) MeV is observed. The same peak for ^{15}B is also found in the neutron removal channel of ^{17}B (see Table I). Note, however, that this peak is in fact a doublet as observed in Ref. [16] (1.327 and 1.407 MeV), which cannot be resolved in Fig. 2(b) because of the experimental resolution. The two transitions can be resolved using γ-γ coincidence as described in Sec. III C1.

Figures 2(c) and 2(d) show the spectra of the γ ray in coincidence with ^{14}B and ^{12}B produced by the neutron removal reactions of ^{17}B, respectively, which can be used to check the energy calibration. These reactions were included in our data and could be analyzed by identifying a charged particle in the exit channel. These observed γ transitions are summarized in Table I.

The γ-ray energies have been determined by fitting peak regions with a Gaussian distribution plus an exponential background. The systematic uncertainty of the energy calibration (3 keV) with the γ sources is included in the quoted uncertainties. The curves in Fig. 2 have been obtained by a simulation using the GEANT code with these energy values fixed, where the spectra are all well reproduced. The measured γ-ray energies in coincidence with ^{12}B are in perfect agreement with the values from a previous measurement [30]. The energy obtained for ^{14}B is consistent with a measurement using fragmentation of ^{36}S on ^{9}Be [16], but disagrees with a measurement using the ^{14}C(^{7}Li,^{7}Be)^{14}B reaction [29]. In the following, the level schemes and angular distributions associated with these γ transitions in ^{17}B and ^{15}B are presented.

B. Results on ^{17}B

1. Level scheme

The observed γ ray is assigned to the decay from the first excited state at $E_x = 1.07$ MeV to the ground state of ^{17}B since no other γ transitions and no γ-γ correlations were observed. It should be noted, however, that we cannot exclude the possible existence of γ rays with energies below the experimental threshold (about 200 keV) and the existence of isomeric states. The experimental level scheme of ^{17}B is compared to theoretical predictions in Fig. 3. SM1 denotes the shell model calculation with the effective interaction PSDWBT [31] using the OXBASH code [32], and SM2 is another shell

TABLE I. Observed γ-ray energies in the inelastic scattering and neutron removal reactions of ^{15}B and ^{17}B on ^{12}C. For ^{15}B, the energy values obtained by assuming a single peak and from the γ-γ coincidence analysis (parenthesis) are shown.

Nuclide	Reaction	This work (MeV)	Previous works (MeV)
^{17}B	^{12}C(^{17}B,^{17}B*)	1.07(1)	
^{15}B	^{12}C(^{17}B,^{15}B*)	1.34(1) [1.30(4), 1.41(2)]	1.327(12), 1.407(20) [16]
	^{12}C(^{15}B,^{15}B*)	1.35(1)	
^{14}B	^{12}C(^{17}B,^{14}B*)	0.652(2)	0.654(5) [16], 0.740(40) [29]
	^{12}C(^{15}B,^{14}B*)	0.655(3)	
^{12}B	^{12}C(^{17}B,^{12}B*)	0.953(4), 1.66(1)	0.95310(60), 1.67352(60) [30]
	^{12}C(^{15}B,^{12}B*)	0.957(4), 1.68(2)	

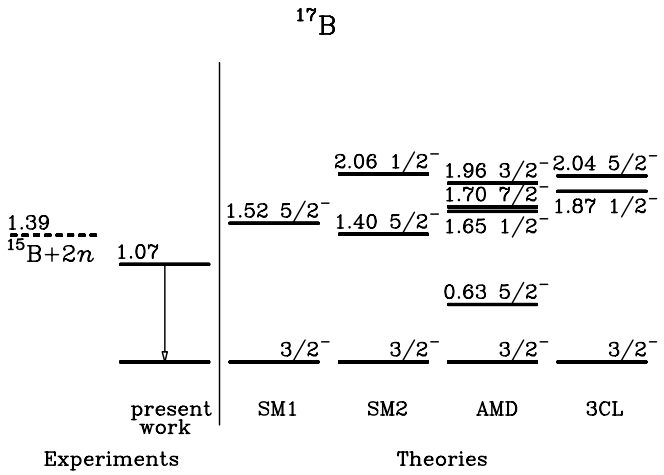

FIG. 3. Level scheme of ^{17}B. The dashed line shows the two neutron separation energy ($S_{2n} = 1.39$ MeV [1]), and the arrow shows the transition observed in this experiment. SM1 and SM2 denote shell model calculations [31,33]. AMD and 3CL denote an AMD prediction [12] and microscopic three-cluster model [7], respectively.

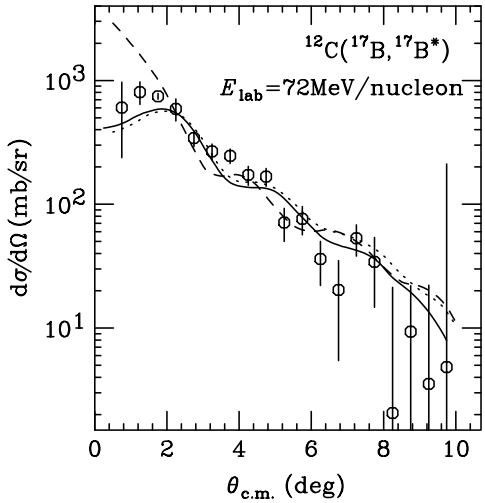

FIG. 4. Angular distribution of inelastically scattered ^{17}B. The solid (dotted) lines show the result of distorted-wave calculations by assuming $\Delta L^\pi = 2^+$ with optical potential parameter set A (B), which are summarized in Table II. The comparison with the $\Delta L^\pi = 1^-$ calculation is shown by the dashed line.

model prediction from Ref. [33]. AMD denotes the calculation by the antisymmetrized molecular dynamics model [12], and 3CL denotes the microscopic three-cluster model [7] where ^{17}B is described as ^{13}B + dineutron + dineutron.

The shell model predictions SM1 and SM2 better reproduce the experimental result compared to AMD and 3CL. The quoted AMD calculations are done with the simplest version, which tends to predict excitation energies too low [34]. All the calculations except 3CL consistently suggest that the first excited state of ^{17}B is $J^\pi = 5/2^-$. Since the energies of the shell models (SM1, SM2) better agree with the experimental one, we adopt here the spin-parity assignment of $5/2^-$ for the observed state for the following analysis.

2. Angular distribution

Figure 4 shows the angular distribution of the inelastic scattering populating the first excited state in ^{17}B. For comparison, the lines show DWBA calculations using the code ECIS97 [35], where the experimental angular resolution is folded.

We use a standard rotational collective excitation model with a $\Delta L^\pi = 2^+$ ($3/2^- \rightarrow 5/2^-$) transition for the DWBA calculation. The calculation was performed using two sets of optical potential parameters: Set A is determined by the ^{12}C + ^{12}C reaction at 85 MeV/nucleon [36] and set B is determined by the ^{16}O + ^{12}C reaction at 94 MeV/nucleon [37], which are listed in Table II.

The calculations with the assumption of $\Delta L^\pi = 2^+$ with these parameter sets (solid and dotted curves) reproduce well the experimental angular distributions, which is consistent with the current $J^\pi = 5/2^-$ assignment for the observed state. However, we could not exclude the possibility of $J^\pi = (1/2, 3/2, 7/2)^-$, which can be excited with $\Delta L = 2^+$, since angular pattern is only sensitive to ΔL. The other possibilities of positive-parity states populated by $\Delta L^\pi = 1^-$ are clearly excluded as shown by the dashed curve in Fig. 4.

The quadrupole deformation length $\delta = \beta R$, where β and R represent, respectively, the deformation parameter and nuclear radius, is obtained from the differential cross section by searching the best fit value with the calculated one using the ECIS code. In the calculation, we assumed $\delta = \delta^{\rm N} = \delta^{\rm C}$ where $\delta^{\rm N}$ and $\delta^{\rm C}$ denote the nuclear and Coulomb deformation lengths, respectively. This assumption does not affect the determination of δ since the nuclear contribution is dominant over the Coulomb contribution for the ^{12}C(^{17}B,^{17}B*) reaction. For instance, the δ value does not change by more than 3% when the $\delta^{\rm C}$ value is set to zero. The angle-integrated cross section for $\theta_{\rm c.m.} \leqslant 10^\circ$ and the extracted deformation lengths of ^{17}B for the two optical potential parameter sets are listed in Table III.

TABLE II. Optical potential parameter sets A and B. Set A is determined by the ^{12}C + ^{12}C reaction at 85 MeV/nucleon [36] and set B is determined by the ^{16}O + ^{12}C reaction at 94 MeV/nucleon [37].

Original reaction	Energy (MeV/nucleon)	V_0 (MeV)	r_v (fm)	a_v (fm)	W_0 (MeV)	r_w (fm)	a_w (fm)	r_c (fm)
^{12}C + ^{12}C (set A) [36]	85	120	0.71	0.84	34.02	0.96	0.69	1.3
^{16}O + ^{12}C (set B) [37]	94	80	0.881	0.763	23.1	1.054	0.825	0.95

TABLE III. Inelastic scattering cross sections populating the first excited state in ^{17}B and the first and second excited states in ^{15}B. The cross sections σ and σ_{DWBA} represent the experimental and calculated cross sections for $0^\circ \leqslant \theta_{\mathrm{c.m.}} \leqslant 10^\circ$, respectively, and δ represents the deduced quadrupole deformation length. A and B denote the optical potential parameter sets used in the analysis.

Nuclide	Transition	σ (mb)	σ_{DWBA} (mb)	δ (fm)
^{17}B	$3/2^-_{\mathrm{g.s.}} \rightarrow 5/2^-_{\mathrm{1st}}$	11.8(2.5)		(A) 1.25(6)
				(B) 1.15(6)
^{15}B	$3/2^-_{\mathrm{g.s.}} \rightarrow 5/2^-_{\mathrm{1st}}$	7.4(3.7)	9.0(1.3)	(A) 1.21(9)
				(B) 1.13(8)
	$3/2^-_{\mathrm{g.s.}} \rightarrow 7/2^-_{\mathrm{2nd}}$	6.3(2.1)	5.1(8)	(A) 1.21(9)
				(B) 1.13(8)

The quoted uncertainties contain both statistical and systematic ones. A systematic uncertainty of 16% due to the γ-ray detection efficiency has been evaluated from the difference between the simulation and the measurement using the ^{22}Na, ^{60}Co, and ^{137}Cs γ sources. By taking an average of the results obtained from the two optical potential parameter sets, a deformation length $\delta = 1.20(8)$ fm for the transition in ^{17}B is adopted in the present work, which will be later compared to shell model predictions and discussed in more detail in Sec. IV.

3. Possibility of spin-flip 1^+ *transition*

In the analysis of the angular distribution, we assumed a pure $\Delta L^\pi = 2^+$ ($\Delta J^\pi = 2^+$, $\Delta L = 2$, $\Delta S = 0$) transition. However, this analysis is valid only if the $\Delta J^\pi = 1^+$ ($\Delta L = 0$, $\Delta S = 1$) spin-flip component, which is allowed to be mixed in the $3/2^- \longrightarrow 5/2^-$ transition, is negligible. In a naive consideration, this mixture is expected to be small since for $\Delta S = 1$ excitation, ^{12}C has to be mutually excited to the 1^+ state. To confirm that this mutual excitation indeed does not affect the current analysis, we estimate the cross section of this spin-flip excitation ^{12}C[^{17}B($3/2^-_{\mathrm{g.s.}}$),^{17}B($5/2^-$)]^{12}C(1^+). For a $\Delta L = 0$, $\Delta S = 1$ reaction, it is known that the cross section of spin flip at zero degrees [$\sigma_{\mathrm{sf}}(0^\circ;^{17}\mathrm{B})$] is proportional to the corresponding $B(M1)$ value. Here, we use this proportionality to compare our case with the zero-degree cross section for ^{12}C[^{12}C,^{12}C(1^+_2)]^{12}C(1^+_2) [$\sigma_{\mathrm{sf}}(0^\circ;^{12}\mathrm{C})$]. The ratio of the cross sections $\sigma_{\mathrm{sf}}(0^\circ;^{17}\mathrm{B})/\sigma_{\mathrm{sf}}(0^\circ;^{12}\mathrm{C})$ is approximately the ratio of $B(M1)$ for the $^{17}\mathrm{B}(3/2^-_{\mathrm{g.s.}}) \rightarrow {}^{17}\mathrm{B}(5/2^-)$ transition to that for the $^{12}\mathrm{C}(0^+_{\mathrm{g.s.}}) \rightarrow {}^{12}\mathrm{C}(1^+_2)$. The $B(M1)$ value for the ^{12}C case is known experimentally to be 0.888 μ_N^2 [38], while for the ^{17}B case it is estimated to be 0.83 μ_N^2 using the shell model with the PSDWBT effective interaction [31]. Hence, $\sigma_{\mathrm{sf}}(\theta = 0^\circ, {}^{17}\mathrm{B})$ is expected to be of the same order as $\sigma_{\mathrm{sf}}(\theta = 0^\circ, {}^{12}\mathrm{C})$. Although the $\sigma_{\mathrm{sf}}(\theta = 0^\circ, {}^{12}\mathrm{C})$ is not known experimentally, it can be estimated using the analogous transition, ^{12}C[^{12}C,^{12}N(1^+)]^{12}B(1^+), which was measured at 135 MeV/nucleon with a zero-degree cross section of about 6 mb/sr [39]. After taking into account the kinematical corrections, we estimate that $\sigma_{\mathrm{sf}}(\theta = 0^\circ, {}^{17}\mathrm{B})$ is of the order of 10 mb/sr. Since the experimental cross section at zero degrees obtained in the present experiment is about 400 mb/sr (see in Fig. 4), we can safely neglect the $\Delta J^\pi = 1^+$ reaction channel.

C. Results on ^{15}B

1. γ-γ coincidences

The peak at 1.35 MeV shown in Fig. 2(b) can be further analyzed using the γ-γ coincidence technique. Figures 5(a) and 5(b) show scatter plots of E_{high} vs E_{low} for two γ-ray coincidence events in the ^{12}C(^{17}B,^{15}B*) and ^{12}C(^{15}B,^{15}B*) reactions, respectively. Here E_{high} and E_{low} denote the higher and lower Doppler-corrected energies of the two observed γ rays.

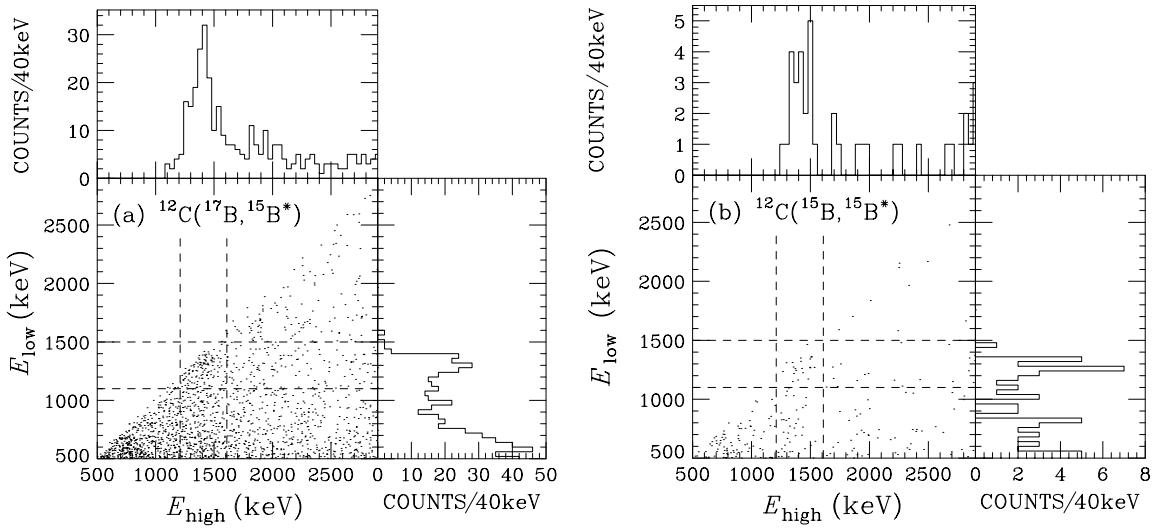

FIG. 5. γ-γ correlations for the (a) ^{12}C(^{17}B,^{15}B) and (b) ^{12}C(^{15}B,^{15}B) reactions. Projected histograms for the bands between dashed lines are also presented. The band regions are 1.10 MeV $\leqslant E_{\mathrm{low}} \leqslant$ 1.50 MeV and 1.21 MeV $\leqslant E_{\mathrm{high}} \leqslant$ 1.61 MeV.

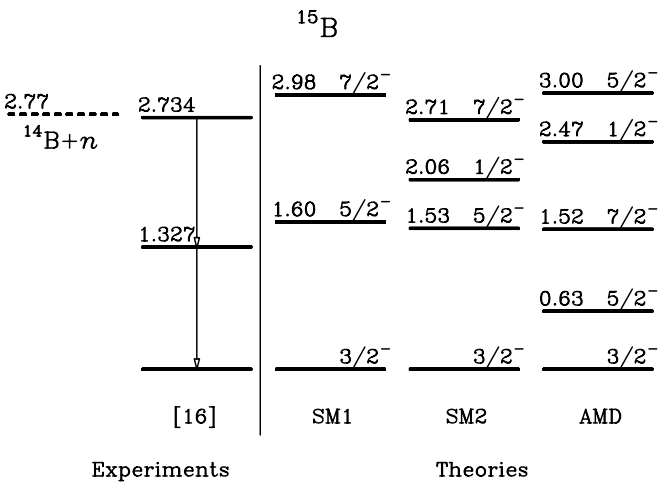

FIG. 6. Level schemes of ^{15}B. The dashed line shows the one neutron decay threshold ($S_n = 2.77$ MeV [14,15]). SM1, SM2, and AMD denote the theoretical predictions same as for ^{17}B.

We confirm the cascade decay from both reactions as apparent in the figures. From the results of the ^{12}C(^{17}B,^{15}B*) reaction [Fig. 5(a)], which has higher statistics, the energies of the two γ rays are 1.30(4) and 1.41(2) MeV as listed in Table I. The energy values are consistent with the recently measured values 1.327 and 1.407 MeV [16], respectively. According to Ref. [16], the observed 1.41 MeV γ ray corresponds to the transition from the second excited state to the first excited state, while the γ ray at 1.30 MeV corresponds to the transition from the first excited state to the ground state.

In Fig. 6, the level scheme of ^{15}B is compared with theories, where SM1, SM2, and AMD are taken from the same references as for ^{17}B.

All of the theories predict the spin-parity of the first excited state to be $5/2^-$, while the spin-parity of the second excited state is predicted to be either $7/2^-$ or $1/2^-$. To assign the spin-parity of the second excited state, we estimated the decay branching ratio from the second excited state using a shell model calculation with SM1 using OXBASH, which reproduces well the experimental level scheme. The calculation predicts $B(E2; 7/2^- \rightarrow 3/2^-) = 6.4\, e^2\,\mathrm{fm}^4$, $B(M1; 7/2^- \rightarrow 5/2^-) = 1.2\, \mu_N^2$, and $B(E2; 7/2^- \rightarrow 5/2^-) = 12\, e^2\,\mathrm{fm}^4$. The second excited state of $J^\pi = 7/2^-$ decays mostly to the first excited state (98%), since the $M1$ transition is fast. This is in sharp contrast with the other possible assignment with $J^\pi = 1/2^-$ which decays directly to the ground state (100%). We also checked that the branching calculated with PSDMK [40] interaction gives the same result, which implies that the choice of the effective interaction has no influence. The observation of the cascade decay in the γ-γ analysis, and the nonexistence of the peak around 2.7 MeV in the energy spectrum for the ^{12}C(^{15}B,^{15}B*) reaction [Fig. 2(b)] and the ^{12}C(^{17}B,^{15}B*) reaction are consistent with the spin-parity assignment of $J^\pi = 5/2^-$ and $7/2^-$ for the first and second excited states, respectively. This assignment is consistent with Ref. [16], where the decay branching ratio was also used for the determination of spin-parities.

To obtain the inelastic cross section for each state, we extracted the number of the first and second excited states ($N_{1\mathrm{st}}$ and $N_{2\mathrm{nd}}$) populated in the inelastic scattering using the relation

$$Y_\gamma^{\mathrm{detec}} = \epsilon_\gamma N_{1\mathrm{st}} + \epsilon_{\gamma\gamma} N_{2\mathrm{nd}}, \tag{1}$$

where $Y_\gamma^{\mathrm{detec}}$ represents the yield of the detected γ rays for multiplicity = 1. The efficiencies ϵ_γ and $\epsilon_{\gamma\gamma}$ are for one and two γ emission with multiplicity = 1, respectively. $N_{2\mathrm{nd}}$ can be extracted independently using the γ-γ coincidence events. $Y_\gamma^{\mathrm{detec}}$ was deduced from the peak yield in Fig. 2(b), and $N_{1\mathrm{st}}$ was then obtained with the relation (1). The cross sections obtained are 7.4(3.7) mb for the transition to the first excited state and 6.3(2.1) mb for the transition to the second excited state as listed in Table III. The uncertainties of the extracted cross sections are large primarily because of the low statistics of the γ-γ coincidence events.

2. Angular distribution

It is difficult to obtain the angular distributions separately for the two excited states because of the low statistics of γ-γ coincidence events. Instead, we analyze the angular distribution associated with the doublet peak in Fig. 2(b) as a whole. Here we define the effective cross section σ_{eff} as

$$\sigma_{\mathrm{eff}} = c Y_\gamma^{\mathrm{detec}} \big/ \epsilon_{\mathrm{eff}}, \tag{2}$$

and

$$\frac{d\sigma_{\mathrm{eff}}}{d\Omega} = c \frac{dY_\gamma^{\mathrm{detec}}}{d\Omega} \frac{1}{\epsilon_{\mathrm{eff}}}, \tag{3}$$

where c is a constant value, which contains the information of the number of incident particles and target thickness, and c is used to convert the γ-ray yield to the cross section. The ϵ_{eff} value is defined as an effective efficiency when we assume that only one γ ray is emitted from ^{15}B. Inserting Eq. (1) into (2) and (3), we obtain

$$\sigma_{\mathrm{eff}} = [\epsilon_\gamma \sigma(\mathrm{g.s.} \rightarrow 1\mathrm{st}) + \epsilon_{\gamma\gamma} \sigma(\mathrm{g.s.} \rightarrow 2\mathrm{nd})]/\epsilon_{\mathrm{eff}}, \tag{4}$$

and

$$\frac{d\sigma_{\mathrm{eff}}}{d\Omega} = \left[\epsilon_\gamma \frac{d\sigma}{d\Omega}(\mathrm{g.s.} \rightarrow 1\mathrm{st}) + \epsilon_{\gamma\gamma} \frac{d\sigma}{d\Omega}(\mathrm{g.s.} \rightarrow 2\mathrm{nd}) \right] \Big/ \epsilon_{\mathrm{eff}}. \tag{5}$$

The experimental effective differential cross section $d\sigma_{\mathrm{eff}}/d\Omega$ for the ^{12}C(^{15}B,^{15}B*) reaction has been obtained using the relation (3) and is shown in Fig. 7.

These are compared to the calculations where $d\sigma_{\mathrm{eff}}/d\Omega$ is extracted using Eq. (5) while calculating $d\sigma/d\Omega$(g.s. $\rightarrow$ 1st) and $d\sigma/d\Omega$(g.s. $\rightarrow$ 2nd) separately by using the following assumptions. With the optical potential parameter sets A and B used for the case of ^{17}B (see Table II), the calculation was done by assuming that the ground state ($J^\pi = 3/2^-$) and the two excited states ($J^\pi = 5/2^-, 7/2^-$) are members of the $K = 3/2$ rotational band of the ground state. With this assumption, a common deformation length δ can be used for the transition to the first and second excited states. We also assume a 100% cascade decay, which is reasonable according to the

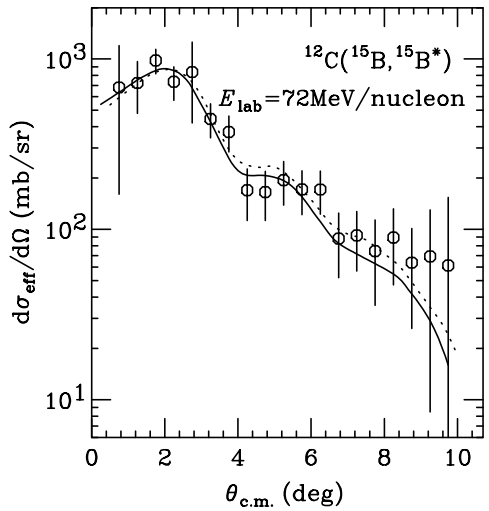

FIG. 7. Angular distribution of inelastically scattered ^{15}B. The Y axis is the effective differential cross section. The solid (dotted) lines show the result of distorted wave calculations with the optical potential parameter set A (B).

shell model calculation mentioned above (98%). The cross sections and deformation length are extracted to reproduce the normalization of the experimental $\sigma_{\rm eff}$ integrated from 0° to 10° in $\theta_{\rm c.m.}$. The difference in the cross section depending on the choice of optical potential parameters is less than 1% and is thus negligible. The extracted deformation lengths δ and the cross sections $\sigma_{\rm DWBA}$ calculated with optical potential set A are summarized in Table III. The calculated cross sections are in good agreement with the ones extracted from the γ-γ coincidence analysis. By taking an average of the results obtained for the two optical potential parameter sets, a deformation length $\delta = 1.17(12)$ fm for the transitions in ^{15}B is adopted in the present work.

The contribution of a possible $\Delta J^\pi = 1^+$ transition was estimated and found negligible as in the case of ^{17}B. The possibility of a $\Delta L^\pi = 1^-$ transition was also examined and excluded as well.

IV. DISCUSSION

The deformation lengths obtained in this experiment are compared with proton and neutron multipole matrix elements M_p and M_n obtained from the shell model. It should be noted that the proton and neutron effective charges e_p and e_n of the nucleus are related to M_p and M_n. Here we use Bernstein's prescription [41,42]

$$\frac{\delta^{\rm probe}}{\delta^{\rm C}} = \frac{1 + (b_n/b_p)(M_n/M_p)}{1 + (b_n/b_p)(N/Z)}, \tag{6}$$

where the deformation length $\delta^{\rm probe}$ is expressed as a function of M_p and M_n. The parameters b_p and b_n represent the interaction strengths of the probe particle with the protons and neutrons of the nucleus. The values of b_p and b_n are characteristic of the probe particle. We assume $b_p = b_n$ for the inelastic scattering on ^{12}C, because ^{12}C is a $T = 0$ probe like ^{4}He. In the rotational model, $B(E2; I_i \to I_f)$ of a rotational K band is related to the Coulomb deformation length $\delta^{\rm C}$ via the equations,

$$B(E2; I_i \to I_f) = Q_0^2 e^2 \frac{5}{16\pi} \langle I_i K 20 | I_f K \rangle^2, \tag{7}$$

$$Q_0 = \left(\frac{16\pi}{5}\right)^{1/2} \frac{3}{4\pi} Z R_0 \delta^{\rm C}, \tag{8}$$

where Q_0 is the intrinsic quadrupole moment. The Coulomb radius R_0 is taken as $1.2A^{1/3}$ fm. From these equations, we derive the following result,

$$\delta^{\rm probe} = \frac{4\pi}{3eR_0} \frac{1}{\sqrt{2I_i+1}} \frac{1}{\langle I_i K 20 | I_f K \rangle} \frac{b_p M_p + b_n M_n}{b_p Z + b_n N}. \tag{9}$$

Note that in the case of odd-even nuclei the additional factor depending on I_i and I_f needs to be included, unlike the case of even-even nuclei [23].

The experimental deformation lengths $\delta = 1.20(8)$ fm for ^{17}B and $\delta = 1.17(12)$ fm for ^{15}B are compared to $\delta^{\rm probe}$ calculated by the shell model with Eq. (9). We first performed the calculations using the two effective interactions PSDWBT [31] and PSDMK [40] with conventional values of effective charges $e_p = 1.3\,e$ and $e_n = 0.5\,e$ for the sd-shell region [43]. The calculations with these two interactions differ only by 6%, and thus the difference is not significant. The calculated values with the PSDWBT interaction for ^{17}B and ^{15}B are 1.78 and 1.85 fm, respectively, which are significantly larger than the experimental ones [1.20(8) and 1.17(12) fm].

The large discrepancy of δ between the experiment and theory may suggest the different effective charges from the conventional ones. In fact, the measurements of the Q moment for ^{15,17}B [8,9] indicated the quenching of the neutron effective charge for these neutron-rich boron isotopes. We examine this quenching of the neutron effective charge for the current results with the proton effective charge $e_p = 1.3\,e$ fixed. Figure 8

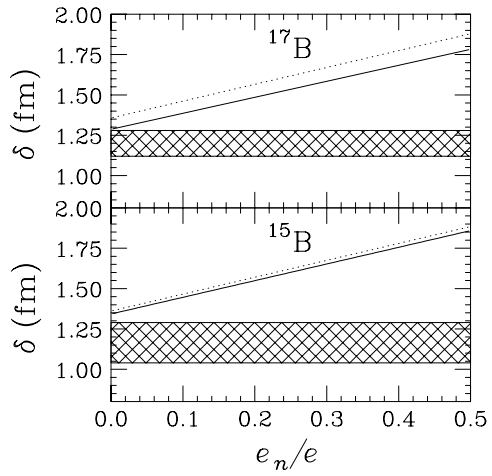

FIG. 8. Dependence of the deformation length δ on the neutron effective charge e_n of ^{17}B (top) and ^{15}B (bottom). Hatched zones indicate the experimental values. The solid and dotted lines show the calculation using the PSDWBT and PSDMK interactions, respectively.

shows the comparison of the experimental deformation lengths with calculated ones as a function of the neutron effective charge e_n. The comparison clearly indicates $e_n \approx 0$, which is consistent with the Q-moment measurements.

This quenching of the neutron effective charge can be considered as an indication of decoupling of the valence neutrons. It should be noted that such a decoupling has been suggested for the neighboring nucleus ^{16}C from recent experimental results [10,11].

V. CONCLUDING REMARKS

Using, in-beam γ-ray spectroscopy with inelastic scattering of the radioactive nuclei ^{15}B and ^{17}B on ^{12}C, we observed a new γ transition in ^{17}B and assigned it as the decay from the first excited state at $E_x = 1.07(1)$ MeV to the ground state. For ^{15}B, we observed two γ transitions, which were assigned as a cascade decay from the second excited state ($E_x = 2.71$ MeV) to the ground state via the first excited state ($E_x = 1.30$ MeV), using a γ-γ coincidence analysis and by comparing the two observed γ-ray energies with those obtained from a recent work using a fragmentation reaction [16]. The advantage of the current experiment using inelastic scattering over the fragmentation is that we can study the transition itself from the ground state to each excited state of the nucleus. With the help of DWBA analysis, we found that the angular distributions exhibit the $\Delta L^\pi = 2^+$ characteristics. The obtained energy levels and their $\Delta L^\pi = 2^+$ characteristics are consistent with the assignment of $5/2^-$ for the first excited state of ^{17}B, and $5/2^-$ and $7/2^-$, respectively, for the first and second excited states of ^{15}B, which are predicted by the shell model using the PSDWBT effective interaction (SM1).

Intriguing results have come out from the further analysis of the transition strengths. The deformation lengths for the transitions in ^{15}B and ^{17}B have been extracted using differential cross sections analyzed with the ECIS code and compared to the shell model calculations. In the ECIS calculation for the ^{15}B transitions, we assumed a macroscopic rotational model, with which the observed angular distribution and the cross sections for the two transitions are well reproduced. The comparison of the deformation lengths with the shell model calculation led to the result that the conventional effective charges $e_p = 1.3\,e$ and $e_n = 0.5\,e$ in the *sd*-shell region cannot reproduce the data; this suggests a strong quenching of e_n for both ^{15}B and ^{17}B. Since such a quenching and the decoupling of valence neutrons are seen not only for ^{15,17}B but also for the neighboring nucleus ^{16}C, there may exist a"region" where such decoupling is particularly strong. From the inelastic scattering and Q-moment measurements for the neighboring nuclei, it would be particularly interesting to locate the boundary of this "decoupling region" and to understand its features.

In this paper, we used shell model calculations for the interpretation of the experimental results. Note, however, that ^{15}B and ^{17}B are expected to have clustering characteristics such as the Li-He cluster of neutron-rich boron isotopes predicted by the AMD calculations [12,34]. Clustering structure in ^{17}B has also been discussed in terms of the neutron-halo Borromean structure [6] and microscopic three-cluster model [7]. The present results are certainly important in testing these interesting clustering models.

In this work, we demonstrated that the inelastic scattering of radioactive nuclei with a ^{12}C target is a very useful tool, where ^{12}C can play a role as a $T = 0$ probe. We recently measured the inelastic scattering of ^{11}Be to unbound states by ^{12}C, where two $\Delta L^\pi = 2^+$ transitions were observed [44]. It would be interesting if these transitions could be studied with a different probe, such as a proton target, which has a different sensitivity on neutron and proton excitations. The combination of different probes could thus be used to deduce independently the M_n and M_p values, as well as the e_n and e_p values. In fact, we have recently learned that a group at RIKEN has measured the proton inelastic scattering of ^{17}B [45].

ACKNOWLEDGMENT

Sincere gratitude is extended to the accelerator staff of RIKEN for their excellent operation of the beam delivery. Fruitful discussions with Z. Elekes and Zs. Dombrádi are appreciated. The present work was supported in part by a Grant-in-Aid for Scientific Research (No.15540257) from the Ministry of Education, Culture, Sports, Science and Technology (MEXT). The support of a 21st Century COE Program at Tokyo Tech "Nanometer-Scale Quantum Physics" by MEXT for Y. Kondo and T. Sugimoto is also acknowledged.

[1] G. Audi *et al*., Nucl. Phys. **A624**, 1 (1997).
[2] T. Suzuki *et al*., Nucl. Phys. **A658**, 313 (1999).
[3] M. G. Saint-Laurent *et al*., Z. Phys. A **332**, 457 (1989).
[4] A. Ozawa *et al*., Phys. Lett. **B334**, 18 (1994).
[5] T. Suzuki *et al*., Phys. Rev. Lett. **89**, 12501 (2002).
[6] Z. Ren, J. Phys. G **20**, 1185 (1994).
[7] P. Descouvemont, Nucl. Phys. **A581**, 61 (1995).
[8] H. Izumi *et al*., Phys. Lett. **B366**, 51 (1996).
[9] H. Ogawa *et al*., Eur. Phys. J. A **13**, 81 (2002).
[10] N. Imai *et al*., Phys. Rev. Lett. **92**, 62501 (2004).
[11] Z. Elekes *et al*., Phys. Lett. **B586**, 34 (2004).
[12] Y. Kanada-En'yo and H. Horiuchi, Phys. Rev. C **52**, 647 (1995).
[13] R. Kalpakchieva *et al*., Eur. Phys. J. A **7**, 451 (2000).
[14] M. A. Hotchkis *et al*., Nucl. Phys. **A398**, 130 (1983).
[15] T. S. Bhatia *et al*., Phys. Lett. **B76**, 562 (1978).
[16] M. Stanoiu *et al*., Eur. Phys. J. A **22**, 5 (2004).
[17] T. Motobayashi *et al*., Phys. Lett. **B346**, 9 (1995).
[18] P. G. Thirolf *et al*., Phys. Lett. **B485**, 16 (2000).
[19] R. W. Ibbotson, T. Glasmacher, P. F. Mantica, and H. Scheit, Phys. Rev. C **59**, 642 (1999).
[20] B. V. Pritychenko *et al*., Phys. Rev. C **63**, 011305(R) (2000).
[21] K. Yoneda *et al*., Phys. Lett. **B499**, 233 (2001).
[22] Z. Dombrádi *et al*., Nucl. Phys. **A727**, 195 (2003).
[23] H. Iwasaki *et al*., Phys. Lett. **B481**, 7 (2000).

[24] Y. Yanagisawa *et al*., Phys. Lett. **B566**, 84 (2003).
[25] H. Iwasaki *et al*., Phys. Lett. **B491**, 8 (2000).
[26] T. Kubo *et al*., Nucl. Inst. Meth. B **70**, 309 (1992).
[27] H. Kumagai *et al*., Nucl. Inst. Meth. A **470**, 562 (2001).
[28] Computer code GEANT, CERN program library.
[29] G. C. Ball *et al*., Phys. Rev. Lett. **31**, 395 (1973).
[30] H. H. Williams *et al*., Phys. Rev. **144**, 801 (1966).
[31] E. K. Warburton and B. A. Brown, Phys. Rev. C **46**, 923 (1992).
[32] B. A. Brown, A. Etchegoyen, and W. D. M. Rae, computer code OXBASH, MSU Cyclotron Laboratory Report No. 524, 1986.
[33] N. A. F. M. Poppelier, L. D. Wood, and P. W. M. Glaudemans, Phys. Lett. **B157**, 120 (1985).
[34] Y. Kanada-En'yo (private communication).
[35] J. Raynal, Coupled channel code ECIS97 (unpublished).
[36] M. Buenerd *et al*., Nucl. Phys. **A424**, 313 (1984).
[37] M.-E. Brandan, Phys. Rev. Lett. **60**, 784 (1988).
[38] U. Deutschmann *et al*., Nucl. Phys. **A411**, 337 (1983).
[39] T. Ichihara *et al*., Phys. Lett. **B323**, 278 (1994).
[40] D. J. Millener and D. Kurath, Nucl. Phys. **A255**, 315 (1975).
[41] A. M. Bernstein, V. R. Brown, and V. A. Madsen, Comments Nucl. Part. Phys. **11**, 203 (1983).
[42] A. M. Bernstein, V. R. Brown, and V. A. Madsen, Phys. Lett. **B103**, 255 (1981).
[43] B. A. Brown and B. H. Wildenthal, Ann. Rev. Nucl. Sci. **38**, 29 (1988).
[44] N. Fukuda *et al*., Phys. Rev. C **70**, 54606 (2004).
[45] R. Kanungo *et al*., Phys. Lett. **B608**, 206 (2005); Zs. Dombrádi *et al*. (in preparation).